VOL. 11, NO. 1, JANUARY 2016 ISSN 1819-6608
ARPN Journal of Engineering and Applied Sciences

www.arpnjournals.com

FINITE ELEMENT ANALYSIS OF FUSION LASER CUTTING ON STAINLESS STEEL-304

A. M. Sifullah, Y. Nukman, M. A. Hassan and A. Hossain
Department of Mechanical Engineering, Faculty of Engineering, University of Malaya, Kuala Lumpur, Malaysia

ABSTRACT

During laser cutting of stainless steel-304 sheet, temporal variation takes place, while stresses are developed. In addition grain refinement and carbide formation is taken place, which initiates heat affected zone (HAZ) that need to identify. Meanwhile, comprehensive simulation of CO_2 laser cutting process of stainless steel-304 sheet is complex as it involves thermo-mechanical problem. Thus, in this study a coupled thermo-mechanical finite element model is developed using ANSYS to predict the temporal variation together with thermal stress and width of (HAZ). Stainless steel-304 sheet of 1mm thickness is used as workpiece and the effects of laser power and speed on HAZ and thermal stress are investigated. In total seven configurations involving four different laser powers and speeds are used and the results of the simulation model have been validated by experiments. The metallurgical changes along the cut surfaces are examined by optical microscope and SEM. The current study shows that maximum temperature is developed close to the heat source and the width of HAZ increases with increase of laser power and decrease with increase of cutting speed. Cracks and dross are observed along the cutting edge, which are more pronounced at the middle of the workpiece due to maximum stress concentration as shown by FE analysis.

Keywords: finite element analysis, laser cutting, heat affected zone, thermal stress, stainless steel-304.

INTRODUCTION

Fusion laser cutting is a thermo-mechanical process, which uses laser beam as heat source. In contrast with a conventional cutting, it is much precise, accurate, cost effective and less time consuming [1]. In fusion laser cutting, there is no direct contact between workpiece and the cutting equipment; hence the chance of material contamination is zero and can cut wide range of material. Highly concentrated heat source is formed during the cutting process, which produces high quality narrow cut kerf and small heat affected zone (HAZ). These characteristics make it suitable for cutting stainless steel-304 having high melting temperature (1450 ^{0}C).

Stainless steel-304 is a corrosion free austenitic steel alloy having high melting temperature (1450^{0}C). Moreover, it contains significant proportion of carbon (0.055%), manganese (1.00%), phosphorus (0.029%), sulphur (0.005%), silicon (0.6%), chromium(18.28%), nickel (8.48%) [2]. Therefore, heating and rapid cooling associated with laser cutting of stainless steel-304 initiates grain refinement, carbide, sulphide and phosphate formation, that is called HAZ [3-5]. The presence of HAZ in stainless steel introduces some undesirable effects such as embrittlement, decrease in weldability and decrease in corrosion and fatigue resistance, etc. On the other hand, during laser cutting the surface of the workpiece is heated by concentrated laser energy in a tiny area, which causes temporal variation and develops thermal stresses. While, the stresses may exceeds the strength of the material causing material defects such as fractures and cracks in the surface. Thus, minimization of HAZ and stress development is desirable in laser cutting.

Many internal and external parameters such as laser type, power, cutting speed, focal position, nature of assist gas, assist gas pressure and material properties influence the laser cutting process [6,7]. Among them the effect of laser power and cutting speed are the most important, because these parameters directly control the heat generation during the cutting process. Hence, it is of great importance to quantify the relationship among thermal stress, HAZ and cutting parameters (laser power and speed) to improve the cut quality and to minimize the HAZ of fusion laser cutting of stainless steel-304.

Due to the complexity of fusion laser cutting different numerical methods have been developed to describe its mechanism. Among them finite element method (FEM) is more suitable for analysing the steady and transient 2D/3D heat flow during laser cutting. The main advantage of FEM is its ability to use different thermal properties to obtain result thoroughly for different laser parameters. Khan and Yilbas (2004) [8] presented a numerical model for thermal stress by using finite element method (FEM) to cut sheet metal. Anderson and Shin (2006) [9] proposed a transient thermal model for laser assisted machining (LAM) and measured the surface temperature of austenitic stainless steel. Germain *et al*. (2007) [10] proposed a simulation model to plot the HAZ profile in AISI 52100 by using commercial FEA software Abaqus/Standard® and validated with experimental result. Sheng et al. (1995) [3] proposed a 2-D FEM model for width of HAZ and validated with experiment. Yilbas *et al*. (2009) [11] used FEM to simulate the stress development during cutting a hole with 15mm dia. The model was simulated by ANSYS and considered the problem as

sequentially coupled unidirectional problem. In this study, an experimentally validated coupled field thermo-mechanical FEM model for fusion laser cutting of stainless steel-304 sheet is introduced, by using Gaussian distributed heat flux to predict the kerf width, HAZ and stress field. Both the simulation and experiment were performed on stainless steel-304 having thickness 1mm and using four different laser powers and speeds as shown in Table-1. Thermocouples were used to measure the temperature of the workpiece, where optical microscope and scanning electron microscope (SEM) were introduced measure the width of HAZ and to analyze the metallurgical and morphological changes along the cutting edge.

EXPERIMENTAL SETUP AND PROCEDURE

In this study AMADA FO-2412 CO_2 laser machine, with AMNC CNC control was used to perform the experiment. Laser beam diameter was 0.40mm, produced by using 127 mm focal lens. Nitrogen, as an assist gas was used and impinged on the workpiece from a conical nozzle at a pressure of 0.9 psi in order to get oxide and burr-free cut [12]. K-type thermocouples (TC-1, TC-2) with data logger were placed to measure the temperature of the workpiece as shown in Figure-1. Both the thermocouples were placed 5mm away from the laser path to avoid high heating of the laser beam. Four different laser powers and speed were used to perform 25mm straight cuts on stainless steel-304 sheet as shown in Table-1. After the cutting, samples were etched by applying 15 ml HCl, 5 ml HNO3, and 100 ml H_2O.[5] The etched samples were examined by an optical microscope and SEM to measure the HAZ and analyse the microstructure analysis.

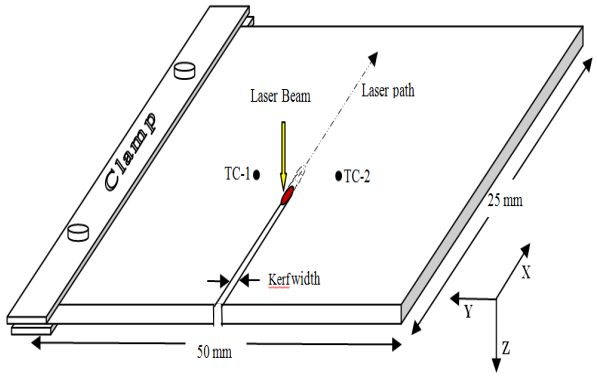

Figure-1. Schematic diagram of experimental setup.

Table-1. Laser cutting parameters used in experiment and simulation.

Experiment No.	Laser power (watt)	Speed (mm/sec)
1	1000	80
2	1200	80
3	1400	80
4	1600	80
5	1600	100
6	1600	120
7	1600	140

FINITE ELEMENT MODEL

Theoretical development

The process of fusion laser cutting is thermal in nature. Whenever the laser beam strikes on the surface of workpiece, a part of the laser energy is absorbed by the material. The absorbed energy then generates heat and creates molten layer. Immediately after that the molten layer is blown out from the workpiece and produces cut kerf. Measuring the absorption capacity of laser is very complex and depends not only on the thermo-optical properties of the material but also on the laser properties (wavelength, frequency, beam polarization etc). From the previous research it is found that the absorption capacity of stainless steel-304 varies from 0.20 to 0.645 [13, 14, 12, 15]. In this study the average value of absorptivity was considered 0.50.

In constructing a theoretical FE model for thermo-mechanical analysis the following assumptions are considered:

1. The laser beam strikes on the surface of the workpiece perpendicularly and it is Gaussian in nature. The Gaussian distribution of absorbed heat flux is expressed by Eq (1).

$$q(x,y) = I_O A \exp\left(-\frac{\left(x^2+y^2\right)}{r^2}\right) \quad (1)$$

where, I_o $P/\pi r^2$, laser intensity in *watt/m*^{2}

P laser beam power in *watt*

A absorption co-efficient

r beam radius in *meter*

2. The material of stainless steel-304 is isotropic and homogeneous.

3. The thermo-mechanical properties of stainless steel-304 considered are shown in Table-2

4. With an appropriate depth of focus, the laser energy density is equal along the thickness of the workpiece.

5. The molten layer of material is removed from the workpiece immediately after melting by assist gas and no vaporization has taken place.

6. The workpiece is clamped, parallel to the cutting line and the effect of assist gas pressure is ignored.

7. There is no effect of cooling by assist gas.

8. The atmospheric temperature is 30^0C.

9. Natural convection is taken place and convection coefficient is considered 30 W/m^2 K.

10. The effect of radiation heat loss is negligible compare to conduction and convection heat transfer. Hence, radiation heat transfer is not considered.

Heat transfer analysis of the model

From the Fourier's law, the mathematical model for time dependant 3D transient heat conduction for laser cutting can be written by Equation (2) [16].

$$\rho c_p\left(\frac{\partial T}{\partial t}+v\frac{\partial T}{\partial x}\right)=\frac{\partial}{\partial x}\left(k\frac{\partial T}{\partial x}\right)+\frac{\partial}{\partial y}\left(k\frac{\partial T}{\partial y}\right)+\frac{\partial}{\partial z}\left(k\frac{\partial T}{\partial z}\right)+Q_{\text{int}} \quad (2)$$

where: k Thermal conductivity ($W\,m^{-1}\,K^{-1}$)
C_p Specific Heat ($J\,Kg^{-1}K^{-1}$)
ρ Density ($Kg\,m^{-3}$)
v Velocity (ms^{-1})
Q_{int} Rate of heat generation (Wm^{-3})
Initial condition of workpiece is explained by Equation (3)

$$T(x,y,z,0) = T_a \quad (3)$$

where: T_a Ambient temperature (30^0C)

Assuming free convection to atmosphere, the general boundary condition at the bottom, top and lateral surfaces are expressed by Equation (4)

$$q_{freeconv} = h_{freeconv}\left(T_s - T_a\right) \quad (4)$$

where:

$h_{freeconv}$ Convective heat transfer coefficient of air (30 $WK^{-1}m^{-2}$)
T_s Surface Temperature (^{0}C)

In laser cutting the workpiece is heated locally by induced laser energy and the temperature of the material is increased. In this study it is assumed that immediately after the melt, the molten material is blown away from the surface with the help of highly pressurized assist gas N_2. Thus the cutting is taken place avoiding further increase in temperature of the material to the boiling temperature and beyond. Based on principle of energy balance and considering one dimensional heat flow during melting, the rate of material removal is calculated [17]. Thus, energy required to melt a mass, m of a material at room temperature is written as [18].

$$E_m = \frac{\pi d^2}{4}\rho v_m t\left[C_s\left(T_m - T_{amb}\right)+L_f\right] \quad (5)$$

where: E_m Energy to melt the material (J)
d Diameter of laser beam (m)
P Density of workpiece ($kg\,m^{-3}$)
v_m Penetration speed (ms^{-1})
t Time (s)
C_s Specific heat of solid($Jkg^{-1}K^{-1}$)
T_m Melting temperature (K)
T_{amb} Atmospheric temperature (K)
L_F Latent heat of fusion (Jkg^{-1})
In addition, the laser power required to melt the material is given by:

$$P_m = AP = \frac{E_m}{t} \quad (6)$$

Therefore, the volume removed per second per unit area (melting speed) is determined by:

$$v_m = \frac{4AP}{\pi d^2 \rho\left[C_S\left(T_m - T_{amb}\right)+L_f\right]} \quad (7)$$

Table-2. Thermo-mechanical properties of stainless steel 304 [19, 20].

Temperature (^{0}C)	**Density** (g cm^{-3})	**Thermal conductivity** (W m^{-1} K^{-1})	**Specific heat** (KJ g^{-1}K^{-1})	**Young's modulus E** (GPa)	**Poisson's ratio** (ν)	**Thermal expansion coefficient** (α×10−6 (K−1))
20	7931	15.5	435	197.13	0.27	16.03
100	7896	16.2	452	194.00	0.28	17.05
200	7849	17.5	479	187.18	0.284	17.54
300	7801	18.9	499	181.00	0.289	18.00
400	7753	20.3	517	170.00	0.291	18.73
500	7704	21.8	534	160.73	0.295	19.36
600	7655	23.4	551	148.00	0.299	19.84
800	7555	26.6	585	125.50	0.302	21.24
1000	7453	29.8	622	69.20	0.305	23.49
1200	7346	33.1	663	20.55	0.32	23.49
1450	7249	36.3	865	8.84	0.32	23.49

Thermal stress analysis

Heat associated with fusion laser cutting is local and concentrated in a small area where the laser beam focused. As the cutting progresses the focused position of laser beam is advancing with time. Thus the heated area cools down sharply after heating due to convection and radial heat conduction. That cause temporal variation and thermal stress is development. The temporal variation ΔT can be described by Eq.8 [8].

$$\sigma_{them} = \frac{E\alpha\Delta T}{1-\upsilon} \quad (8)$$

Where: E Young's modulus
α Thermal expansion coefficient
v Poisson's ratio

The equivalent von Mises stress is given by the following expression:

$$\sigma_m = \sqrt{\frac{(\sigma_1-\sigma_2)^2+(\sigma_2-\sigma_3)^2+(\sigma_1-\sigma_3)^2}{2}} \quad (9)$$

where σ_1, σ_2, σ_3 are the three principal stresses from any point in the x, y, or z directions of the principal axis obtained from Eq. 9. Plastic deformation takes place when σ_m reaches the yield strength of the material.

Solution procedure

In this study commercial finite element software ANSYS is used to simulate the proposed thermo-mechanical model considering sequentially coupled field analysis technique. In this technique the results of thermal analysis (temperature distribution) are considered as input for the structural analysis (thermal stress) as shown in Figure-2.

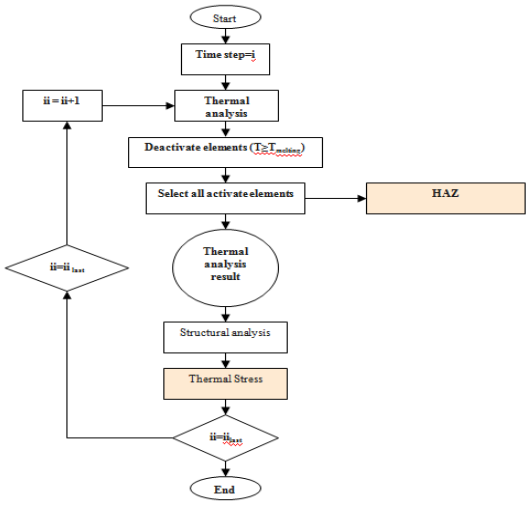

Figure-2. Flow diagram of sequential coupled field analysis in ANSYS.

The laser beam strikes on X-Y plane and travels along the X-axis while the penetration takes place along Z axis (Figure-1). As the cutting is performed along the symmetrical X-axis of the workpiece, hence, half of the workpiece is modelled to reduce the computational time. So the dimension of the workpiece considered in

simulation is 25mm x 12.5mm x 1mm (X x Y x Z). Considering same meshing, two different types of elements are considered for thermal and mechanical analysis. For transient thermal analysis 8 node brick type thermal element SOLID70 is used and an equivalent structural element SOLID45 is employed in structural analysis. The summery of the elements can be found in [21].

The results of FEM analysis depends on mesh density of the model. Because, the coarseness of mesh can produce erroneous result, while too fine mesh size can increase the computational time. In this study mesh convergence parametric studies are done to select the appropriate element size 0.05mm X 0.02mm along the laser path. Non-uniform meshes are used to discretize the model. Fine meshes are considered in the region near the laser path, while less fine meshes in the neighbouring zone of the fine meshes; and coarse meshes in the outer portion of the plate as shown in Fig 3. Total number of elements and nodes were 407380 and 414380 respectively.

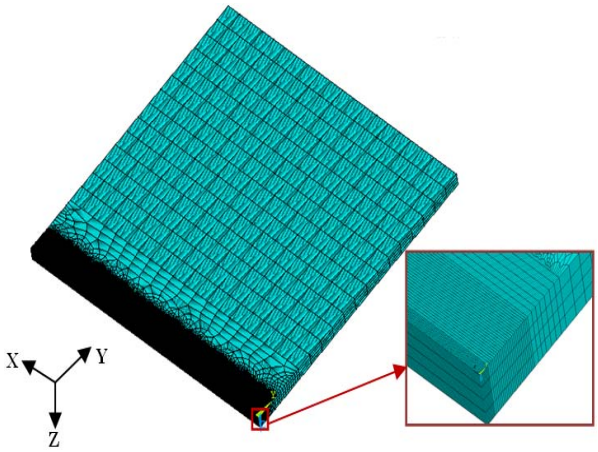

Figure-3. FE Model for analysis.

The movement of the heat flux vector is simulated by using a time varying multiple load steps. Gaussian heat flux is formulated by using ANSYS APDL programming language. Using local co-ordinate system the heat flux is programmed in such a way that it moves on X-Y plane with cutting speed, v and simultaneously penetrates into the workpiece along Z co-ordinate with a melting speed, v_m. Element death methodology (EKILL), available in ANSYS is used to simulate the material removal process during laser cutting. In this methodology, at the end of each time step the elements which cross the melting points (1450^0C) are selected and deactivated (EKILL) (i.e., with insignificant effect in the remaining load steps by setting the conductance to approximately zero) [21]. Hence, in the simulation the temperature of the cutting edge is maintained close to the melting temperature (1450^oC) of stainless steel-304 for all cutting parameters as shown in Figure-4.

Stainless steel-304 is austenitic, imbedded chromium makes it corrosion free. But at 400 ^{0}C - 800 ^{0}C the imbedded chromium turns in to chromium carbide which form HAZ [22,3]. Hence, in the simulation distance upto 800 ^{0}C nodal temperatures are measured and considered as HAZ as shown in Fig-5. In this study HAZ is calculated from the centre of the laser beam by using Eq.10.

Width of HAZ = Kerf width + 2*HAZ associated with remaining workpiece. (10)

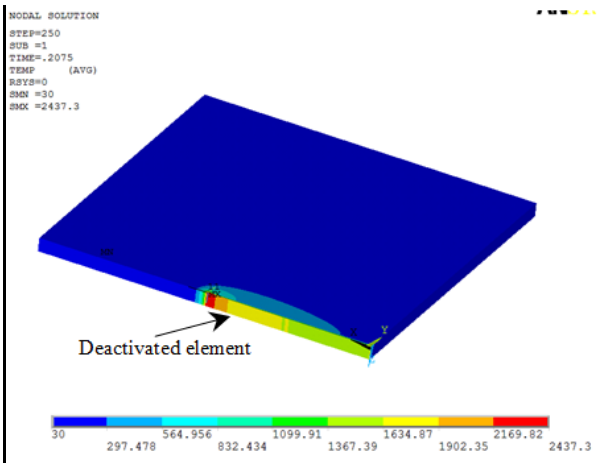

(a)

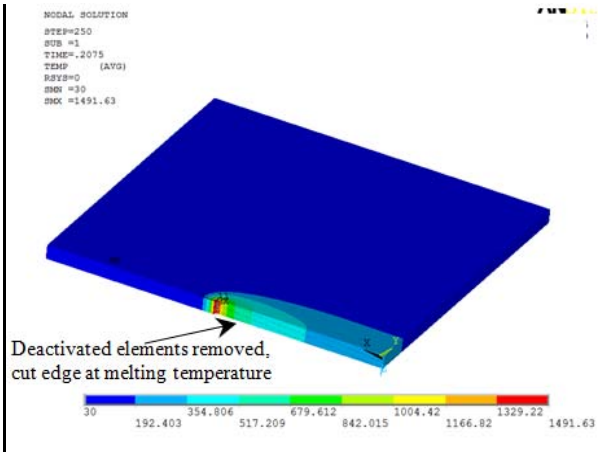

(b)

Figure-4. 3D view of cutting simulation (a) Before removal of deactivated element, (b) After removal of deactivated element.

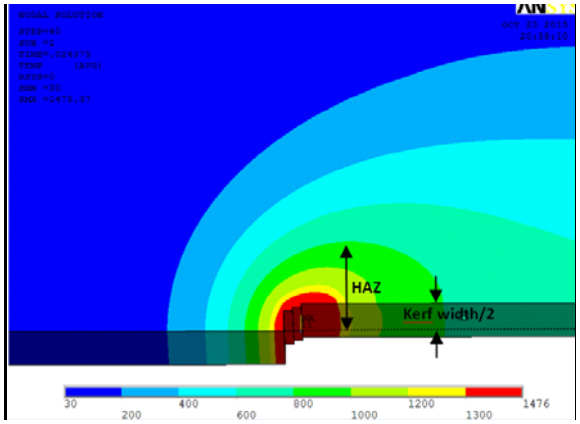

Figure-5. HAZ estimation from simulation.

RESULTS AND DISCUSSIONS

In this study thermo-mechanical FE simulation model is developed to describe the fusion laser cutting on stainless steel-304 sheet. The proposed model is validated by experiment and the effect of laser power and cutting speed on thermal distribution, HAZ and thermal stress fields are analysed.

The 3D view of temperature profile of laser cutting is shown in Figure-4, while the laser power was 1600 watt and cutting speed was 80 mm/sec. It shows that temperature along the Y-axis goes down gradually with the increase of distance as shown in Figure-6.

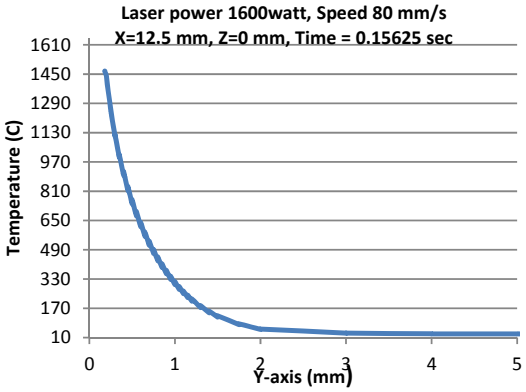

Figure-6. Temperature distribution along the Y-axis.

Figure-7 shows the decay rate of temperature changes with time at the beginning, middle and end of cutting process. It is observed that at the cutting edge the maximum temperature is obtained, which is close to melting temperature 1450 ^{0}C. Immediately after reaching the maximum temperature it goes down sharply and later gradually due to heat loss. The peak temperature at the end of material is higher than the previous stage due to poor heat conduction at the boundary of the workpiece. For every laser cutting same kind of temperature variations are observed.

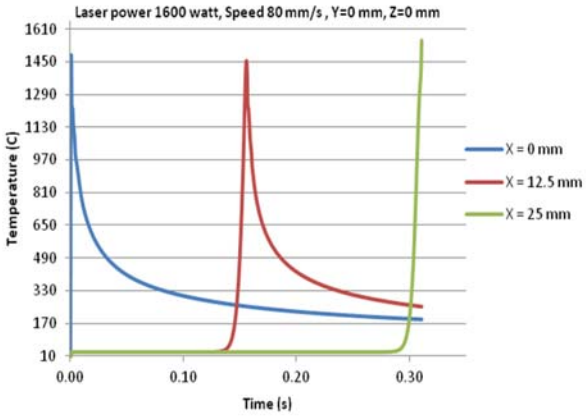

Figure-7. Temperature variation along the kerf at different location.

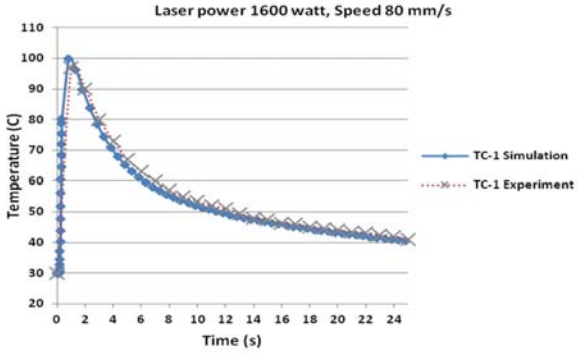

Figure-8. Time temperature curve; comparison between experiment and simulation result at a point 5 mm away from laser path.

During experiment, K-type thermocouples were placed 5 mm away from the laser path to record the temperature. Figure-8 shows the comparison of experimental and simulation results of temperature change with time at the same location (5mm away from laser path). After the cutting the workpiece was cooled at the atmospheric condition up to 25 sec to reach the normal temperature. The experimental and simulation results show good agreement with each other.

The contribution of laser parameters (laser power and speed) on HAZ is identified by doing a parametric study as shown in Figure-9. Keeping all other parameters unchanged the laser cutting were performed by using four different laser powers (1600 watt, 1400 watt, 1200 watt and 1000 watt) and four different cutting speeds (80 mm/s, 100 mm/s, 120 mm/s and 140 mm/s). The simulation results show good agreement with the

experimental results. Figure-9 shows that by increasing the cutting speed, the HAZ decreases while the laser power 1600 watt. On the other hand, the HAZ increases as laser power increases, while the cutting speeds remain 80 mm/s.

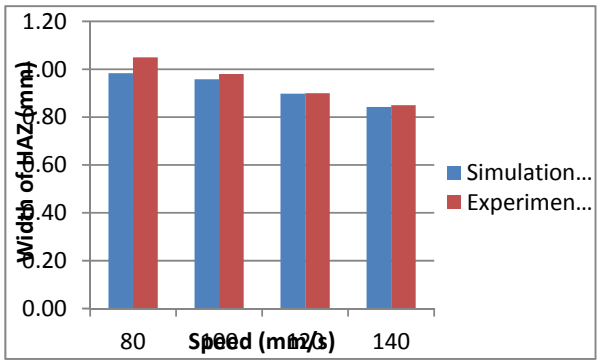

(a)

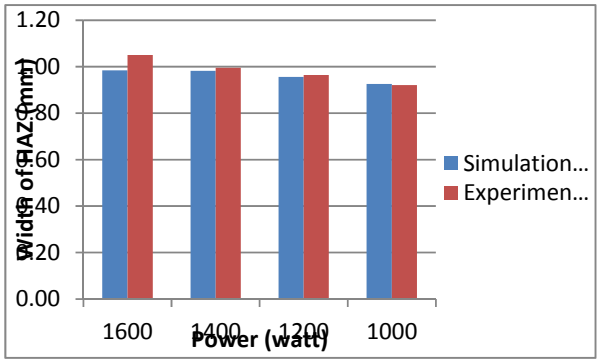

(b)

Figure-9. Comparison of experimental and simulation results of HAZ at (a) different cutting speed (power 1600 watt), different laser power (cutting speed 80mm/s).

Thermal stress in laser cutting is developed due to temporal variation. In this study the thermal stress was analysed by considering the maximum laser power (1600 watt and minimum cutting speed 80 mm/s). Fig-10 shows the temporal variation of von-misses stress of different locations at the cutting edge of material. As the material is constrained to expand at both ends, the highest level of stress intensity was observed at the middle of the workpiece (X=12.5 mm).

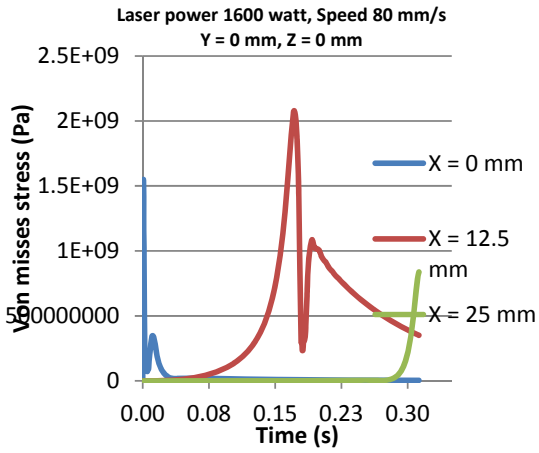

Figure-10. Temporal variations of von-misses stresses of different locations at cutting edge.

Figure-11 shows the cutting samples. It is shown that after etching corrosion was taken place near the kerfwith which indicate the presence of HAZ. Moreover some dross-attachments, cracks and surface defects were observed at the cutting edge. It is may be due to temporal variation which cases thermal stress development to exceed the strength of material. More surface defects are associated with cut kerf, which is at the middle of the workpiece. It is due to more stress development at the middle of the workpiece during the cutting.

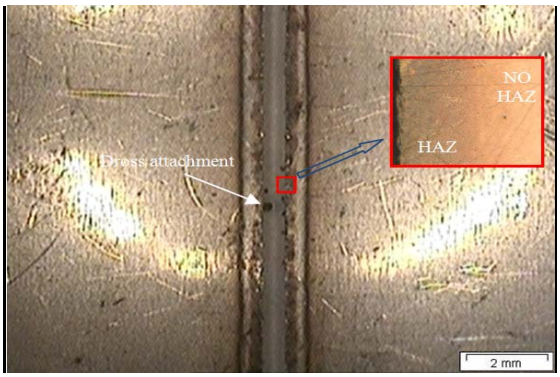

(a)

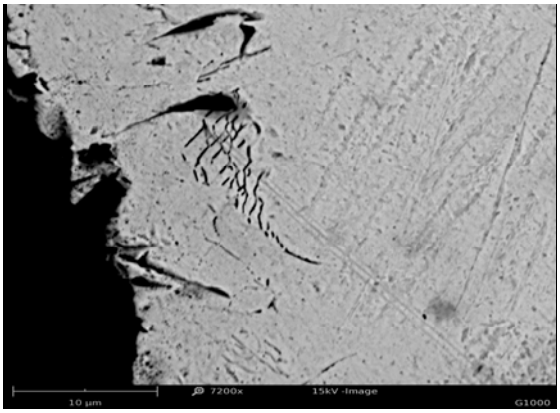

(b)

Figure-11. Images of cutting samples (a) HAZ under optical microscope (b) Cracks under SEM.

CONCLUSIONS

Fusion laser cutting of 1 mm thick stainless steel-304 sheet was performed by using finite element simulation to predict the width of HAZ. The outcomes of simulated model were validated by experiment. ANSYS APDL was used to simulate the Gaussian heat source and element death mythology was employed for material removal. The proposed thermo-mechanical simulation was a combination of thermal and structural (mechanical) analysis. From the thermal analysis, HAZ was measured and temperature distribution during laser cutting was analysed. The simulation outcomes of thermal analysis show that the width of HAZ increases with an increase in laser power and decreases with an increase in cutting speed. Moreover the temperature rises sharply near the focused laser beam. However, thermal gradient decreases sharply and gradually with the increase of distance from the cutting edge. From the structural analysis the outcomes of thermal stress was identified. It was found that maximum stress concentrations were observed at the cutting edge especially at the middle of the workpiece which was supported by the analysis of optical microscope and SEM

ACKNOWLEDGEMENTS

Financial and technical supports from the University of Malaya under the grant RP010C-13AET (UMRG) are gratefully acknowledged.

REFERENCES

[1] Yusoff N, Ismail SR, Mamat A, Ahmad-Yazid A. 2008. Selected Malaysian Wood CO2-Laser Cutting Parameters and Cut Quality. American Journal of Applied Sciences. 5 (8):990.

[2] Shanmugam NS, Buvanashekaran G, Sankaranarayanasamy K, Manonmani K. 2009. Some studies on temperature profiles in AISI 304 stainless steel sheet during laser beam welding using FE simulation. The International Journal of Advanced Manufacturing Technology. 43(1-2):78-94. doi: 10.1007/s00170-008-1685-0.

[3] Sheng PS, Joshi VS. 1995. Analysis of Heat-Affected Zone Formation for Laser Cutting of Stainless-Steel. Journal of Materials Processing Technology. 53(3-4):879-892. Doi: 10.1016/0924-0136(94)01761-O.

[4] Masumoto I, Shinoda T, Hirate T. 1990. Weld Decay Recovery by Laser Beam Surfacing of Austenitic Stainless Steel Welded Joints. Transactions of the Japan Welding Society. 21(1):11-17.

[5] Jamshidi Aval H, Farzadi A, Serajzadeh S, Kokabi AH. 2009. Theoretical and experimental study of microstructures and weld pool geometry during GTAW of 304 stainless steel. The International Journal of Advanced Manufacturing Technology. 42 (11-12): 1043-1051. doi:10.1007/s00170-008-1663-6.

[6] Chen S-L. 1999. The effects of high-pressure assistant-gas flow on high-power CO 2 laser cutting. Journal of Materials Processing Technology. 88(1):57-66.

[7] Wang J. 2000. An experimental analysis and optimisation of the CO2 laser cutting process for metallic coated sheet steels. The International Journal of Advanced Manufacturing Technology. 16 (5): 334-340.

[8] Khan OU, Yilbas B. 2004. Laser heating of sheet metal and thermal stress development. Journal of materials processing technology. 155:2045-2050.

[9] Anderson M, Shin Y. 2006. Laser-assisted machining of an austenitic stainless steel: P550. Proceedings of the Institution of Mechanical Engineers, Part B: Journal of Engineering Manufacture. 220(12): 2055-2067.

[10] Germain G, Morel F, Lebrun J-L, Morel A. 2007. Machinability and surface integrity for a bearing steel and a titanium alloy in laser assisted machining (optimisation on LAM on two materials). Lasers in Engineering. 17 (5):329.

[11] Yilbas BS, Arif AFM, Aleem BJA. 2009. Laser cutting of holes in thick sheet metals: Development of stress field. Optics and Lasers in Engineering. 47(9): 909-916. doi:http://dx.doi.org/10.1016/j.optlaseng.2009.03.002

[12] Steen WM, Mazumder J, Watkins KG. 2003. Laser material processing. Springer.

[13] Boyden S, Zhang Y. 2006. Temperature and wavelength-dependent spectral absorptivities of metallic materials in the infrared. Journal of thermophysics and heat transfer. 20(1):9-15.

[14] Mazumder J, Steen W. 1980. Heat transfer model for CW laser material processing. Journal of Applied Physics 51 (2):941-947.

[15] C.W. Tan YCC, Leung, N.W. Bernard, Tsun, John, C.K. Alex. 2005. Characterization of Kovar-to-Kovar laser welded joints and its mechanical strength. Optics and Lasers in.

[16] Engineering. 43:151-162.

[17] Yang J, Sun S, Brandt M, Yan W. 2010. Experimental investigation and 3D finite element prediction of the heat affected zone during laser assisted machining of Ti6Al4V alloy. Journal of Materials Processing Technology 210(15): 2215-2222. doi:http://dx.doi.org/10.1016/j.jmatprotec.2010.08.007.

[18] Steen W. 1991. Laser material processing. Springer, London.

[19] Radovanovie M. 2006. Some possibilities for determining cutting data when using laser cutting. Strojniski Vestnik. 52 (10):645-652.

[20] Lee HT, Chen CT. 2011. Numerical and Experimental Investigation into Effect of Temperature Field on Sensitization of AISI 304 in Butt Welds Fabricated by Gas Tungsten Arc Welding. Materials transactions. 52 (7): 1506-1514.

[21] Shiue R, Chang C, Young M, Tsay L. 2004. The effect of residual thermal stresses on the fatigue crack growth of laser-surface-annealed AISI 304 stainless steel: Part I: computer simulation. Materials Science and Engineering: A 364 (1): 101-108.

[22] Inc A. 2007. ANSYS Theory Manual, Release. 11.

[23] Yan J, Gao M, Zeng X. 2010. Study on microstructure and mechanical properties of 304 stainless steel joints by TIG, laser and laser-TIG hybrid welding. Optics and Lasers in Engineering. 48(4): 512-517. doi:http://dx.doi.org/10.1016/j.optlaseng.2009.08.009.